Polybenzimidazole Nanofiltration Hollow Fiber for Cephalexin Separation

Kai Yu Wang and Tai-Shung Chung
Dept. of Chemical and Biomolecular Engineering, National University of Singapore, Singapore 119260

DOI 10.1002/aic.10741
Published online December 19, 2005 in Wiley InterScience (www.interscience.wiley.com).

Most conventional nanofiltration (NF) hollow-fiber membranes are fabricated by means of multiple steps of posttreatments. Because of the unique amphoteric characteristics of the imidazole group in polybenzimidazole (PBI), a novel PBI NF hollow-fiber membrane with appropriate charge characteristics has been fabricated by a one-step phase-inversion process without posttreatment. The resultant mechanically stable PBI membranes can withstand pressures up to 30 bars. It is found that the mean effective pore size decreases, whereas the pure water permeability increases with an increase in elongational draw ratio. The novel PBI NF hollow-fiber membrane exhibits higher rejection to divalent cations, lower rejection to divalent anions, and the lowest rejection to monovalent ions at pH 7.0. Thus the divalent and monovalent ions of both NaCl/$MgCl_2$ and NaCl/Na_2SO_4 binary salt solutions can be effectively fractionated by the PBI NF membrane arising from ion competition. The surface charge characteristics of the PBI NF membrane are strongly dependent on pH. Therefore, by adjusting the pH of cephalexin aqueous solution to modify the ionization states of these dipolar cephalexin molecules, PBI NF membranes show high separation effectiveness for the recovery of this antibiotic from solution over a wide range of pH values. © 2005 American Institute of Chemical Engineers *AIChE J,* 52: 1363–1377, 2006

Keywords: PBI, hollow fiber, macrovoids, nanofiltration, membrane separation, cephalexin

Introduction

During the past decade, nanofiltration has become very important for the liquid-phase separation of a wide range of mixtures or solutions. As one type of pressure-driven membrane separation processes, nanofiltration (NF) falls in between reverse osmosis and ultrafiltration with respect to the characteristics of permeate flux and separation performance.[1] NF membranes have nominal molecular weight cutoffs (MWCO, molecular weight of solute that is 90% rejected by the membrane) ranging from 200 to 1000 Da in the rejection of neutral solutes by their porous-selective layer with estimated pore sizes of around 0.5–2 nm. Moreover, most NF membranes are either negatively or positively charged by the dissociation of surface functional groups, such as sulfonic or carboxyl acids, the adsorption of ions from solution, and the adsorption of polyelectrolytes.[2] Charged membranes are widely used because they can selectively partition ions in the salt mixture solutions through the electrostatic interaction between ions and membrane. Thus, the separation mechanisms, which involve a steric (size exclusion) effect and electrostatic partitioning interaction (Donnan exclusion) between membrane and external solution,[3,4] make nanofiltration an effective means for a wide range of mixture separations containing neutral or charged organic molecules, or electrolytes. Major applications of nanofiltration include removing hardness and dissolved organics from water,[5,6] arsenic removal from drinking water,[7] demineralization in the dairy industry,[8] removal of small organic molecules from the organic synthesis membrane reactor,[9,10] and especially in the purification and separation of pharmaceuticals from fermentation broths.[11]

Correspondence concerning this article should be addressed to T.-S. Chung at chencts@nus.edu.sg.

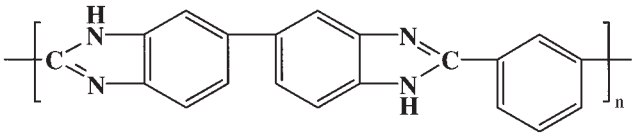

Figure 1. Chemical structure of polybenzimidazole.

The importance of using nanofiltration in the pharmaceutical separation process has been fully recognized. This is explained by the fact that the molecular weights of most pharmaceuticals range from 300 to 1000 Da, which are in the scale of nanofiltration. Generally, pharmaceutical synthesis frequently produces intermediate reaction mixtures in an organic solvent or aqueous solution. The subsequent separation and purification processes to extract valuable intermediate products from these mixtures are crucial to increase product quality and yield.[12] Because most pharmaceutics are thermally labile, special conditions are required to separate these mixtures if one uses conventional separation processes (that is, crystallization, distillation, ion-exchange, and chromatography).[13] Because the membrane-based filtration can be operated at the ambient temperature or lower, nanofiltration would be the preferred separation method for the pharmaceutical syntheses. Nanofiltration has been adopted in the separation of amino acids and peptides from solutions.[14-16]

Since Mahon[17] proposed using hollow-fiber membranes as separation apparatus in his patents four decades ago, synthetic polymeric hollow-fiber membranes have advanced as a key player in separation technologies. Compared to the flat-sheet membrane, the hollow-fiber configuration has the following advantages: (1) a much larger membrane area per unit volume of membrane module, thus resulting in a higher productivity; (2) self-mechanical support, which can be back-flushed for liquid separation; and (3) good flexibility and easy handling during module fabrication and system operation. Nowadays, hollow fibers are widely used in gas separation, reverse osmosis, ultrafiltration, pervaporation, dialysis, and supported liquid membrane extraction.[18,19] However, most available nanofiltration modules are still made in flat-sheet, spiral-wound, and tubular configurations. In addition, most NF membranes are composite membranes by sophisticated fabrication processes. Some of them are fabricated by coating an ultrathin porous barrier layer on a microporous support, whereas others are made through the interfacial polymerization by simultaneously crosslinking a nascent film at the interface or through chemical modification of surface with the aid of sulfonation or carboxylation.[20] There is an urgent need to develop simple and direct spinning technologies to fabricate NF membranes in one step.

The desirable NF membranes for liquid separation must have the following characteristics: (1) suitable porosity to keep a large volume permeate flux; (2) appropriate pore sizes and a narrow pore size distribution to meet the separation requirements; (3) robust mechanical strength to withstand high pressures, and (4) necessary chemical stability to withstand various environments during the operation. However, most polymeric membranes often proved inadequate with respect to chemical resistance to survive in harsh environments with different pH ranges.[21] The purpose of this work is to explore whether polybenzimidazole (PBI) NF hollow-fiber membranes can be developed to meet these harsh requirements. To our best knowledge, no PBI NF hollow fibers have been reported.

Polybenzimidazole is a generic name of a class of heterocyclic polymers. The most common one is poly-2,2′-(*m*-phenylene)-5,5′-bibenzimidazole (PBI) as illustrated in Figure 1. It has a very high glass-transition temperature of approximately 425–435°C attributed to its rigid chain structure.[22] In addition to impressive moisture affinity (absorbing water up to 13 wt %), PBI is known to possess outstanding thermal, physical, and chemical stabilities over a wide range of pH values. However, the uniqueness of PBI for NF membranes is its imidazole group (pK_a 7.2). The group consists of two nitrogen atoms. The nitrogen associated with the hydrogen atom is a hydrogen bond donor, whereas the nitrogen associated with the lone pair is a proton acceptor.[23] PBI can become charged in aqueous environments if the adjacent benzene ring delocalizes the proton of the imidazole group.[24] By using the same principle, acid-doped PBI and sulfonated PBI have been developed for fuel cell applications with superior electrochemical characteristics and excellent solvent resistance.[25-27] Because most NF membranes have pore sizes in the molecular range and are either negatively or positively charged to obtain desirable separation performance, one may be able to harness the advantage of PBI charge characteristics to directly develop PBI NF membranes with little postmodification.

Therefore, the objectives of this article are (1) to study the fabrication of PBI NF hollow-fiber membranes with outstanding mechanical stability to withstand high transmembrane pressures, (2) to determine the charge characteristics of PBI NF hollow fibers and their ion separation performance, and (3) to investigate its application for the separation of cephalexin. Cephalexin, a semisynthetic cephalosporin, is therapeutically advantageous and important for its broad antibacterial activity. Cephalexin is a zwitterionic molecule containing amino group and carboxyl group and is synthesized either by the reduction of phenylglycyl 7-ACA (7-aminocephalosporanic acid) with amino acid esters or by the chemical or enzymatic acylation of 7-ADCA (7-amino 3-deacetoxycephalosporanic acid).[28] Similar to amino acids, the ionization states of cephalexin mole-

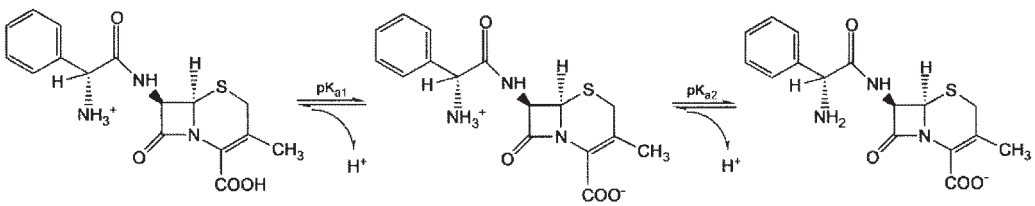

Figure 2. Ionization states of cephalexin at different pH values.

pK_{a1} = 2.56, pK_{a2} = 5.88.

Table 1. Diffusivities and Stokes Radii of Neutral Solutes in Aqueous Solutions (at 20°C)

Solute	MW or M_W (g mol^{-1})	D_s* ($\times 10^{-9}$ m^2 s^{-1})	r_s (nm)
Glycerol	92	0.78	0.260
Glucose	180	0.57	0.365
Saccharose	342	0.43	0.471
Raffinose	504	0.35	0.584
PEG1000	1000	0.21	0.784

*D_s of glycerol = 0.78×10^{-9} m^2 s^{-1}.

cules vary with pH in the aqueous solution, as shown in Figure 2. The traditional solvent extraction cannot be used to recover it from fermentation broths. Reactive extraction by means of liquid membranes was therefore developed.[29] Based on the interaction between ionized cephalexin molecules and charged membrane, nanofiltration could become a potential tool to separate and purify the cephalexin aqueous solution by adjusting pH values.

Theoretical Background of the Solute Transport Method to Characterize the Mean Effective Pore Size and Pore Size Distribution

Nanofiltration membranes have molecular-scale pores on their selective layer that determine the permeate flux and sieving performance. Characterizing the mean pore size and pore size distribution of the newly developed PBI NF membranes by means of the following solute transport method provides essential structural information to predict separation performance.

It has been found that the solute rejection for synthetic membranes can be expressed by a log-normal probability function of solute size, as described in the following equation[30]:

$$R_T = \mathrm{erf}(y) = \frac{1}{\sqrt{2\pi}} \int_{-\infty}^{y} e^{-(u^2/2)} du$$

where

$$y = \frac{\ln r_s - \ln \mu_s}{\ln \sigma_g} \tag{1}$$

where R_T is the solute rejection; r_s is the solute radius; μ_s is the geometric mean radius of solute at $R_T = 50\%$; and σ_g is the geometric standard deviation about μ_s, defined as the ratio of r_s at $R_T = 84.13\%$ and $R_T = 50\%$. When the solute rejection of a membrane is plotted vs. solute radius on the log-normal probability coordinates, a straight line is obtained as

$$F(R_T) = A + B(\ln r_s) \tag{2}$$

By ignoring influences of the steric and hydrodynamic interaction between solute and pores on the solute rejection, the mean effective pore radius (μ_p) and the geometric standard deviation (σ_p) can be assumed to be the same as μ_s and σ_g, respectively.[31] Therefore, based on μ_p and σ_p, the pore size distribution of an NF membrane can be expressed as the following probability density function[32]:

$$\frac{dR_T(r_p)}{dr_p} = \frac{1}{r_p \ln \sigma_p \sqrt{2\pi}} \exp\left[- \frac{(\ln r_p - \ln \mu_p)^2}{2(\ln \sigma_p)^2} \right] \tag{3}$$

where r_p is the effective pore radius of the membrane. The values of μ_p and σ_p determine the position and sharpness of the distribution curves, respectively. This approach had been used to evaluate the mean pore size, the pore size distribution, and the porosity of ultrafiltration membranes based on the solute rejection data of polyethylene glycol (PEG) with different M_w values.[33]

Solutions (200 ppm) containing glycerol, glucose, saccharose, raffinose, or PEG1000 were used to measure the solute rejection (R_T) because the relationship between Stokes radius r_s and molecular weight MW or M_w of these known solutes can be expressed by the following equation[34]:

$$\log r_s = -1.4854 + 0.461 \log MW \tag{4}$$

where r_s and MW are in nm and g mol^{-1}, respectively. This equation can also be used to back-calculate the MW of a hypothetical solute at a given radius.

Experimental

Chemical materials

The PBI polymer solution was purchased from Hoechst Celanese Corp. (Somerville, NJ), with the composition of PBI

Table 2. Spinning Conditions of PBI Hollow-Fiber Membranes from PBI Dope Solution*

	Batch I	Batch II**	Batch III	Batch IV	Batch V
Dope flow rate (mL min^{-1})	1.2 (A), 2.4 (B), 3.6 (C), 3.6 (D)	1.2 (A), 2.4 (B), 3.6 (C), 3.6 (D)	1.0 (A), 2.0 (B), 4.0 (C), 8.0 (D)	2.0 (A), 4.0 (B), 4.0 (C), 4.0 (D), 4.0 (E)	1.0 (A), 4.0 (B), 4.0 (C)
Bore fluid composition	DMAc 86 wt %, H_2O 14 wt %	Dodecane	Ethylene glycol 80 wt %, DMAc 20 wt %	Ethylene glycol 50 wt %, DMAc 50 wt %	Ethylene glycol 23.3 wt %, DMAc 76.7 wt %
Bore fluid flow rate (mL min^{-1})	0.75, 1.5, 2.25, 2.25	0.36, 0.72, 1.08, 1.08	0.25, 0.5, 1.0, 2.0	0.5, 1.0, 1.0, 1.0, 1.0	0.25, 1.0, 1.0
Ratio of dope/bore fluid rate	1.6	3.33	4.0	4.0	4.0
Air gap (mm)	10	10	10	16	20
Take-up speed (m min^{-1})	5.2, 10.7, 10.7, 21.8	3.2, 4.0, 4.9, 20.9	1.8, 4.0, 8.5, 17.4	5.7, 12.2, 18.5, 25.3, 38.4	6.0, 12.9, 26.2

* PBI 21.6 wt %, DMAc 76.7 wt %, LiCl 1.7 wt %. Coagulant bath: tap water, 26°C; dope temperature: 26°C; bore fluid temperature: 26°C. Letters in parentheses correspond to the sample number in Figures 4–7. Air gap: the distance between the spinneret outlet and the top surface of the coagulation bath. Take-up speed: the speed of collecting hollow fibers.
**Refer to Model et al.[55]

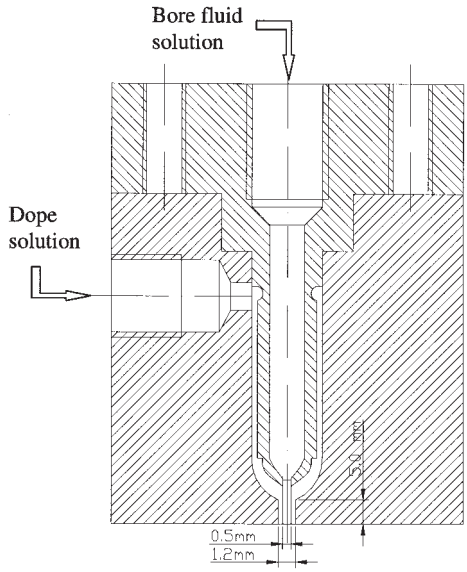

Figure 3. Hollow-fiber spinning spinneret.

25.6 wt %, DMAc 72.4 wt %, and LiCl 2.0 wt %. The intrinsic viscosity of PBI is 0.75 dL/g. The LiCl serves the function of preventing PBI polymer from phasing out of the solution. *N*,*N*-Dimethylacetimide (DMAc), ethylene glycol, and dodecane were purchased from Merck (Darmstadt, Germany). Uncharged neutral solutes of glycerol, glucose, saccharose, raffinose, and PEG1000 (Aldrich, Milwaukee, WI) and several analytical-grade salts, NaCl, $MgCl_2$, $MgSO_4$, and Na_2SO_4 (Merck), were used to characterize membrane structure parameters. Molecular weight, diffusivities, and Stokes radii of these solutes are shown in Table 1.[35] NaOH (1.0 N) and HCl (1.0 N) solutions were used to modify the pH of feed solutions. Cephalexin ($C_{16}H_{17}N_3O_4S{\cdot}H_2O$, MW 365.4, a white crystalline powder) was purchased from MP Biomedicals (Heidelberg, Germany). All chemicals were used as received. The ultrapure water used in all experiments was produced by a Milli-Q unit (MilliPore, Milford, MA) with a resistivity of 18 MΩ cm.

Fabrication of PBI nanofiltration hollow-fiber membranes

The polymer solution of PBI/DMAc/LiCl (21.6/76.7/1.7 wt %) was prepared by diluting the supplied PBI solution with DMAc. Different bore fluid solutions were adopted, such as dodecane, DMAc and water mixture, and DMAc and ethylene glycol mixtures. Table 2 lists the detailed spinning parameters. The schematic diagram of the hollow-fiber spinning spinneret is illustrated in Figure 3. The as-spun hollow fibers were immersed in water for 3–5 days to remove the residual DMAc or/and ethylene glycol. Then, the hollow fibers were post-treated by dipping in a 50 wt % glycerol aqueous solution for

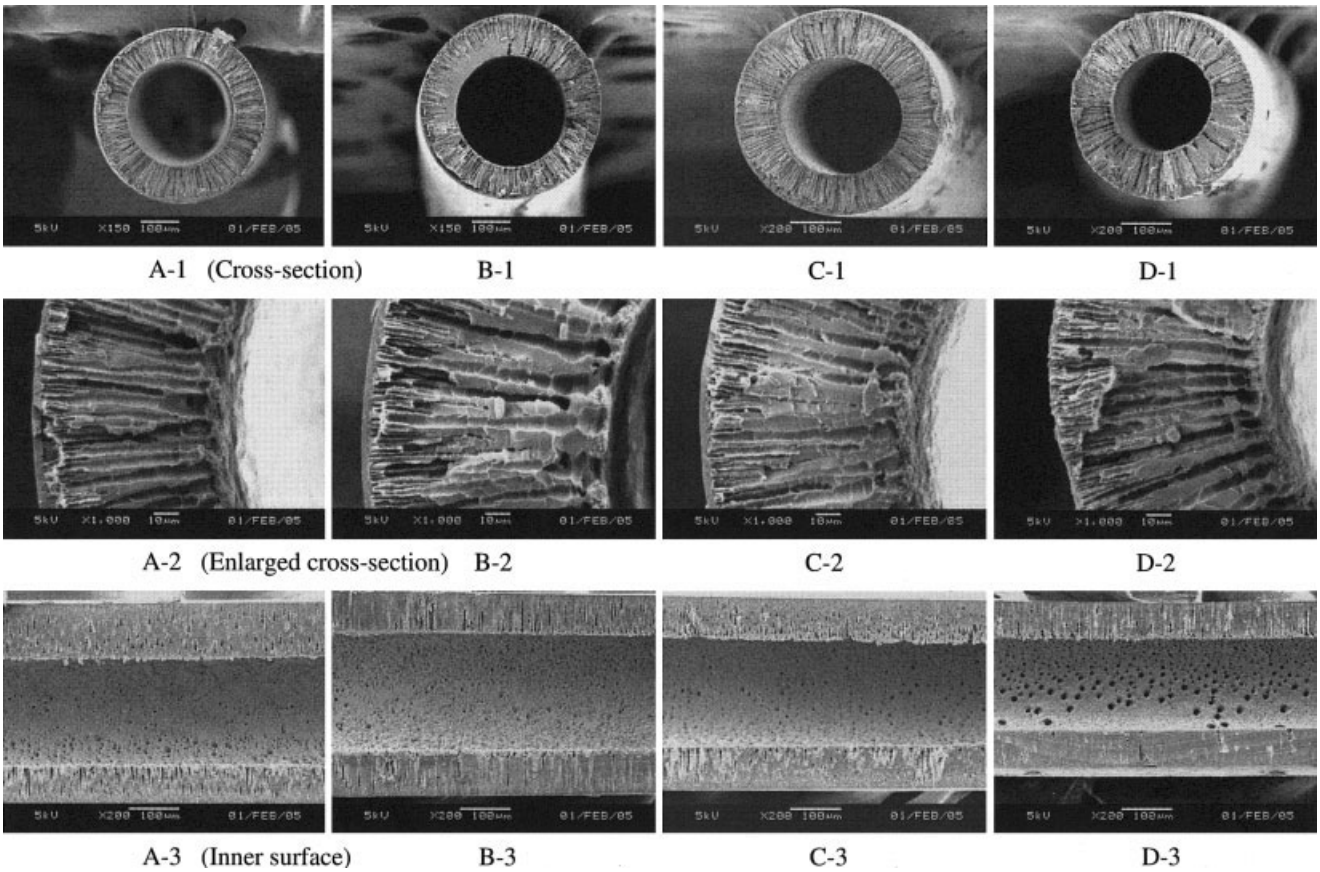

Figure 4. Effects of dope flow rate and elongation rate on the membrane structure of PBI NF hollow-fiber membranes from Batch I.

Bore fluid: DMAc 86 wt %, water 14 wt %.

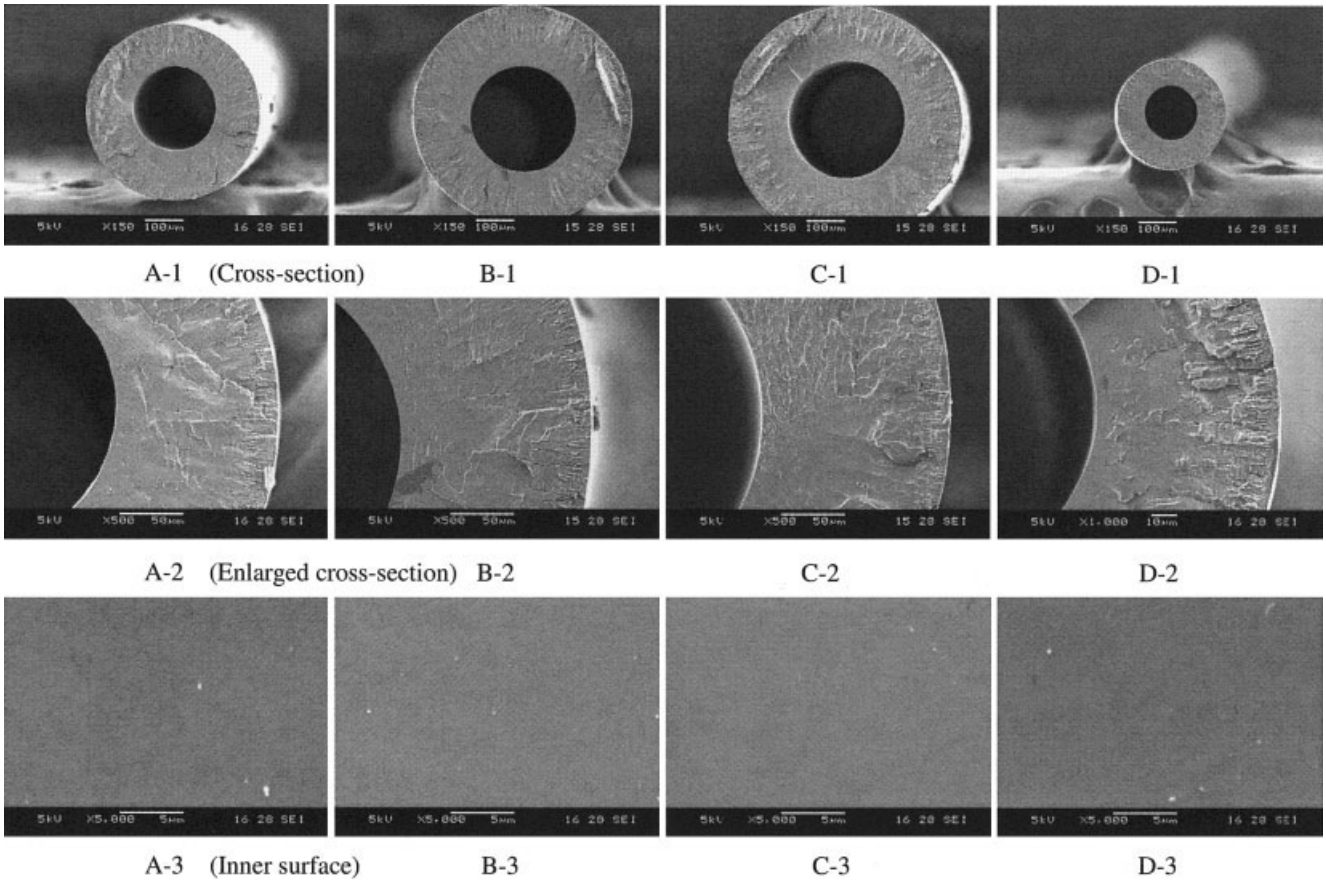

Figure 5. Effects of dope flow rate and elongation rate on the membrane structure of PBI NF hollow-fiber membranes from Batch II.

Bore fluid: dodecane.

48 h and dried in air at room temperature. The dried hollow fibers were used to make hollow-fiber modules for separation experiments.

Extraneous elongational stretching on the spinning line was performed during dry-jet wet spinning in Batch IV. The elongational draw ratio φ is defined as the ratio of the cross-sectional area of dope flowing channel in the spinneret to the solid cross-sectional area of the precipitated hollow-fiber membrane as follows:

$$\varphi = \frac{(\mathrm{OD}^2 - \mathrm{ID}^2)_{spinneret}}{(\mathrm{OD}^2 - \mathrm{ID}^2)_{hollow\ fiber}} \tag{5}$$

The elongational draw ratio is a function of the take-up speed during spinning where extraneous stretching may take place and reduce the dimensions of the hollow fiber. The effect of elongational ratio on the permeate flux and pore size on the selective outer layer will be discussed later.

Chemical analysis

The concentrations of neutral solute and cephalexin solutions were measured with a total organic carbon analyzer (TOC ASI-5000A, Shimadzu, Kyoto, Japan). The concentrations of single electrolyte solutions were measured with an electric conductivity meter (Pioneer30, Radiometer, Neuilly-Plaisance, France). The concentrations of different ions in electrolyte mixtures were measured with ion-selective electrodes (Na^+ or Cl^- combination electrodes, Orion, New Hyde Park, NY). The pH of solution was measured by a pH meter (Orion PerpHect pH meter 370). The dried hollow-fiber membranes were immersed in liquid nitrogen and fractured, and then coated with platinum using a JFC-1100E ion sputtering device (JEOL, Tokyo, Japan). The surface and cross-sectional morphology were observed under a scanning electron microscope (FESEM, JEOL JSM-6700).

Nanofiltration experiments with PBI nanofiltration hollow-fiber membranes

Nanofiltration experiments were conducted in a lab-scale circulating filtration unit, described elsewhere.[36] Two testing modules with filtration area about 100 cm^2 were tested for each hollow-fiber sample. Because the outer surface was the selective layer, the feed was pumped into the shell side and the permeate came out from the fiber lumen, forming a cross-flow filtration mode. The as-spun PBI hollow-fiber membranes were conditioned under different pressures (from 5 to 30 bar depending on their individual mechanical strengths). Then, each membrane sample was first subjected to the pure water filtering to

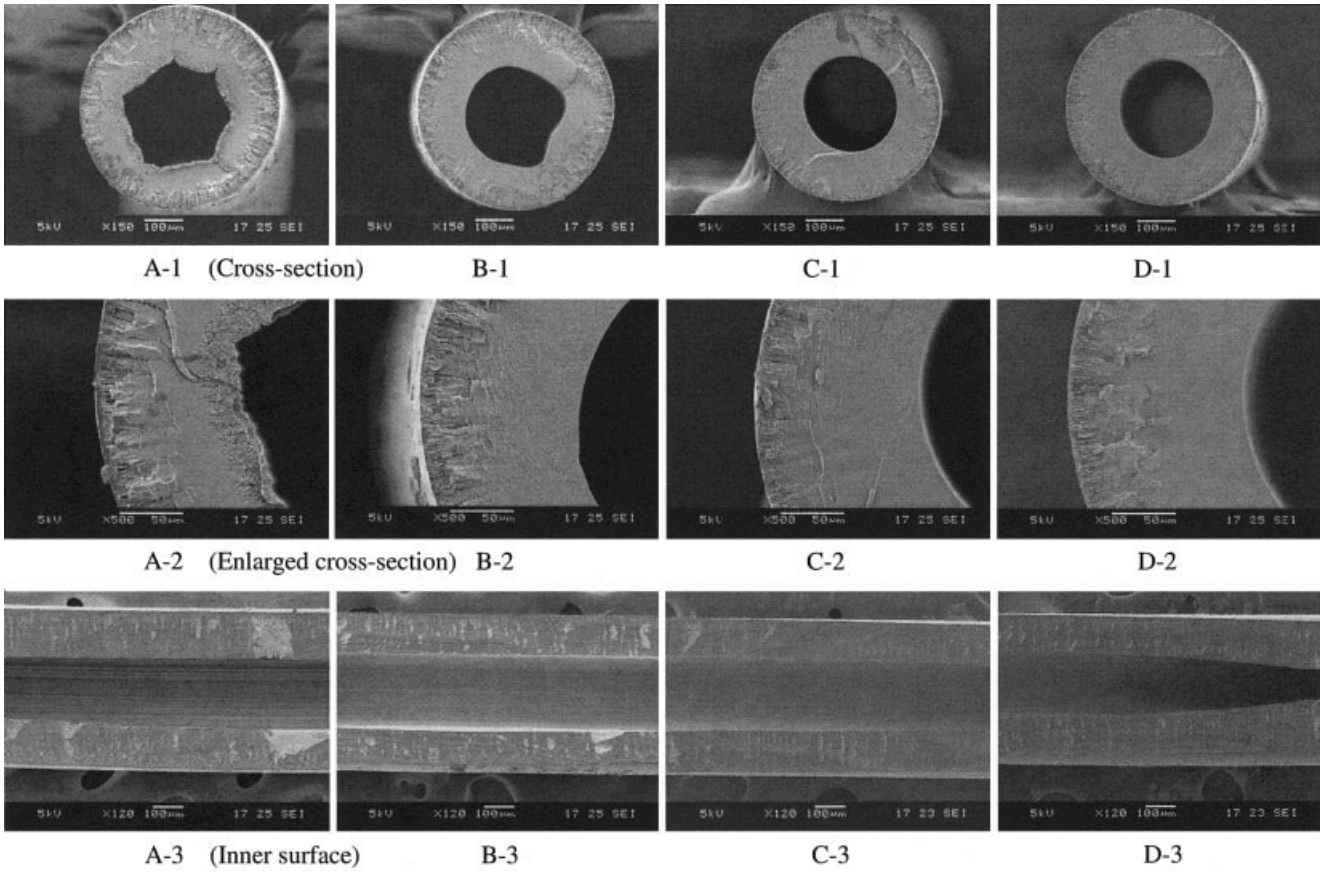

Figure 6. Effects of dope flow rate and elongation rate on the membrane structure of PBI NF hollow-fiber membranes from Batch III.

Bore fluid: ethylene glycol 80 wt %, DMAc 20 wt %.

measure its pure water permeability (PWP, $m^3\ m^{-2}\ kPa^{-1}\ s^{-1}$) under different pressures by[37]

$$\mathrm{PWP} = \frac{Q}{\Delta P \cdot A} \tag{6}$$

where Q is the water permeation volumetric flow rate ($m^3\ s^{-1}$), A is the effective filtration area (m^2), and ΔP is the transmembrane pressure drop (kPa).

Second, the mean effective pore size and the pore size distribution of the membrane samples were characterized according to the solute transport method. Different solutions containing neutral solutes, inorganic salts, and salt mixtures were used in the solute separation experiments. The apparent solute separation coefficient R_T (%) was calculated using the following equation:

$$R_T = \left(1 - \frac{C_{permeate}}{C_{feed}}\right) \times 100 \tag{7}$$

where $C_{permeate}$ and C_{feed} are the solute concentration in the permeate and the feed solutions, respectively.

The feed velocity u_f was selected and kept at about 0.8 m s^{-1}, which could minimize the effect of concentration polarization. This velocity was appropriate because the apparent rejection of studied solutions was very close to the intrinsic rejection (that is, the difference is $<5\%$) and the permeate flux was close to the pure water permeability. The temperature of feed solutions in all experiments was maintained at 20 ± 0.1°C by a cooling coil (controlled by a water circulator, model F32-MV, Julabo Labortechnik GmbH, Seelbach, Germany) inside the feed tank. Each transport experiment was repeated three times and the average was calculated for further analysis.

The following describes experimental designs and separation procedures:

(1) The feed solutions were prepared by dissolving neutral solutes in ultrapure water with a concentration of about 200 ppm. The feed solutions were circulated for about 0.5 h until the whole system reached the steady state where the permeate flux and solute rejection keep unchanged. The permeate was collected for a predetermined period and the volume flux was measured at different pressures (starting from the lowest ΔP).

(2) The nanofiltration experiments were conducted with solutes of progressively higher molecular weights. The membrane was thoroughly flushed with ultrapure water between runs of different solutes. The solute separation data were further used for the estimations of the mean effective pore size and pore size distribution of the membrane.

(3) The electrolyte solutions were prepared by dissolving single salts in ultrapure water with the concentration of 3.4 mol

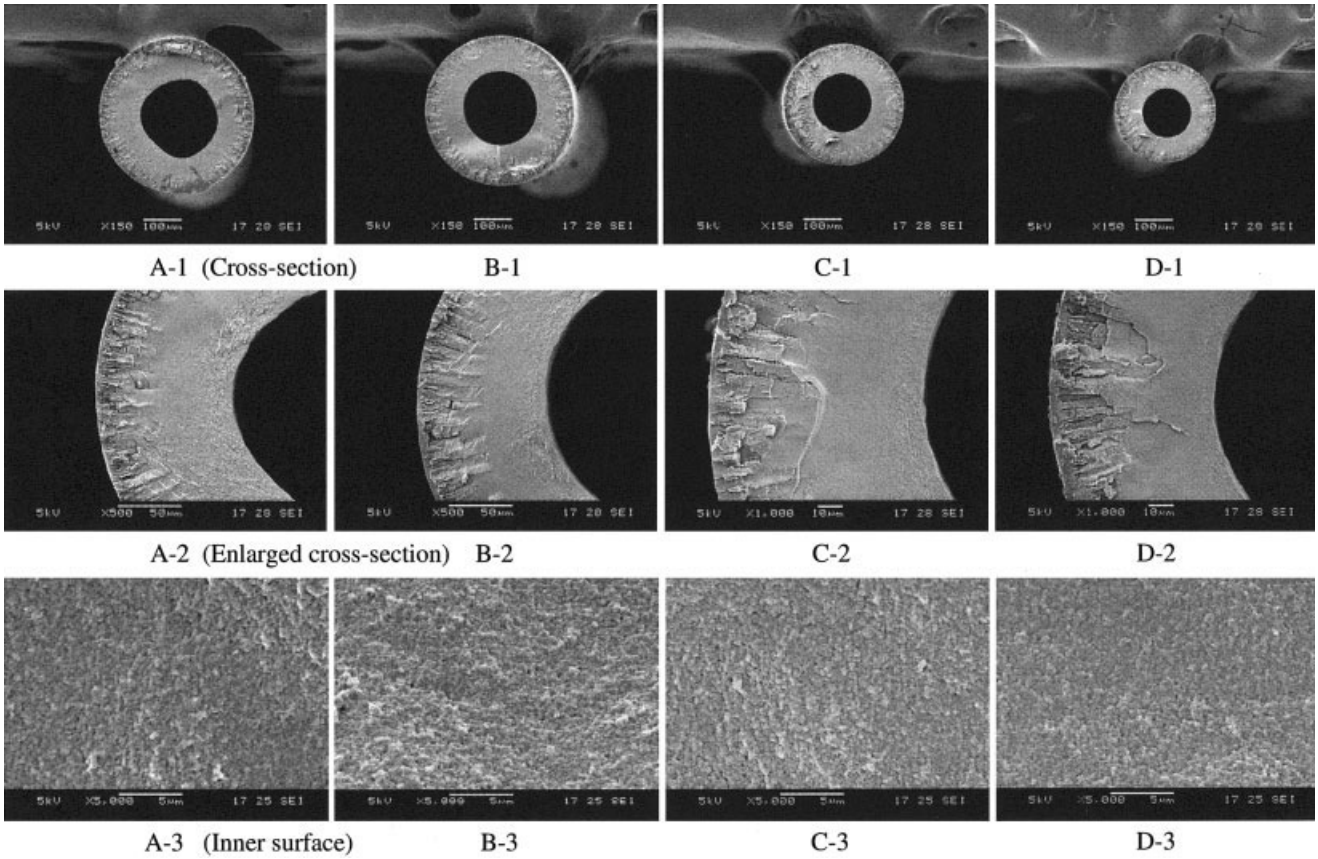

Figure 7. Effects of dope flow rate and elongation rate on the membrane structure of PBI NF hollow-fiber membranes from Batch IV.

Bore fluid: ethylene glycol 50 wt %, DMAc 50 wt %.

m^{-3}. The same experimental procedures were used to measure the salts' rejection performance as described in Step 1.

(4) The $NaCl/MgCl_2$ and $NaCl/Na_2SO_4$ binary salt mixture solutions were prepared at pH 7.0. The ion fractionation performance of membranes was measured at different pressures.

(5) NaCl solutions with different pH were prepared with the concentration of 3.4 mol m^{-3}. The ion rejection by membranes was measured at different pressures.

(6) Cephalexin solutions at different pH values were prepared with a concentration of 200 ppm. The solute rejection experiments were performed according to the same procedure as described in Step 1.

Results and Discussion

Effects of spinning conditions on morphology and strength of PBI NF hollow fibers

The first criterion of NF hollow fibers is to withstand high operating pressures. One of the keys to strengthen membrane compression properties is to reduce the numbers and sizes of macrovoids or increase the ratio of outer diameter (OD) to inner diameter (ID).

Macrovoids in asymmetric hollow fibers have been considered as mechanical weak points that usually result in membrane failure under high pressures. There are many types of macrovoids, such as fingerlike and teardrop macrovoids. The causes of their origins have been debated in the last four decades. Recently, some papers have summarized these debates.[38,39] In short, macrovoids may originate from thermodynamic aspects of chemical potential[40,41] or start from local surface instability and material and stress imbalances, which induce solvent intrusion and capillary flow.[42-44] Other factors such as Marangoni effects[43,46] and osmosis pressure[47] have also been proposed. Ways to reduce macrovoids have received significant attention. Some of them are (1) using high polymer concentration solutions,[48] (2) the addition of high-viscosity components,[49] (3) spinning at high shear rates,[50] (4) the induction of delayed demixing[51] or gelation,[52] (5) the addition of surfactants,[53] and (6) the use of elongational stretch along the spinning line.[39,54]

Different spinning conditions and bore fluid chemistry were used to prepare PBI NF hollow fibers. The objectives are not only to study their effects on membrane structure and separation performance, but also to find proper conditions to minimize macrovoids and to produce NF hollow fibers that can endure high operating pressures. When an 86/14 DMAc/water (weight ratio) mixture was used as the bore fluid, Figure 4 shows the resultant hollow fibers full of long fingerlike macrovoids across the whole cross section. Interestingly, the large and long fingerlike macrovoids were connected through the inner layer pores as shown in the bottom of Figure 4. This cross-sectional morphology may result from the combined effects of a high bore-fluid flow rate, a soft inner skin induced by the delayed demixing arising from the 86/14 DMAc/water

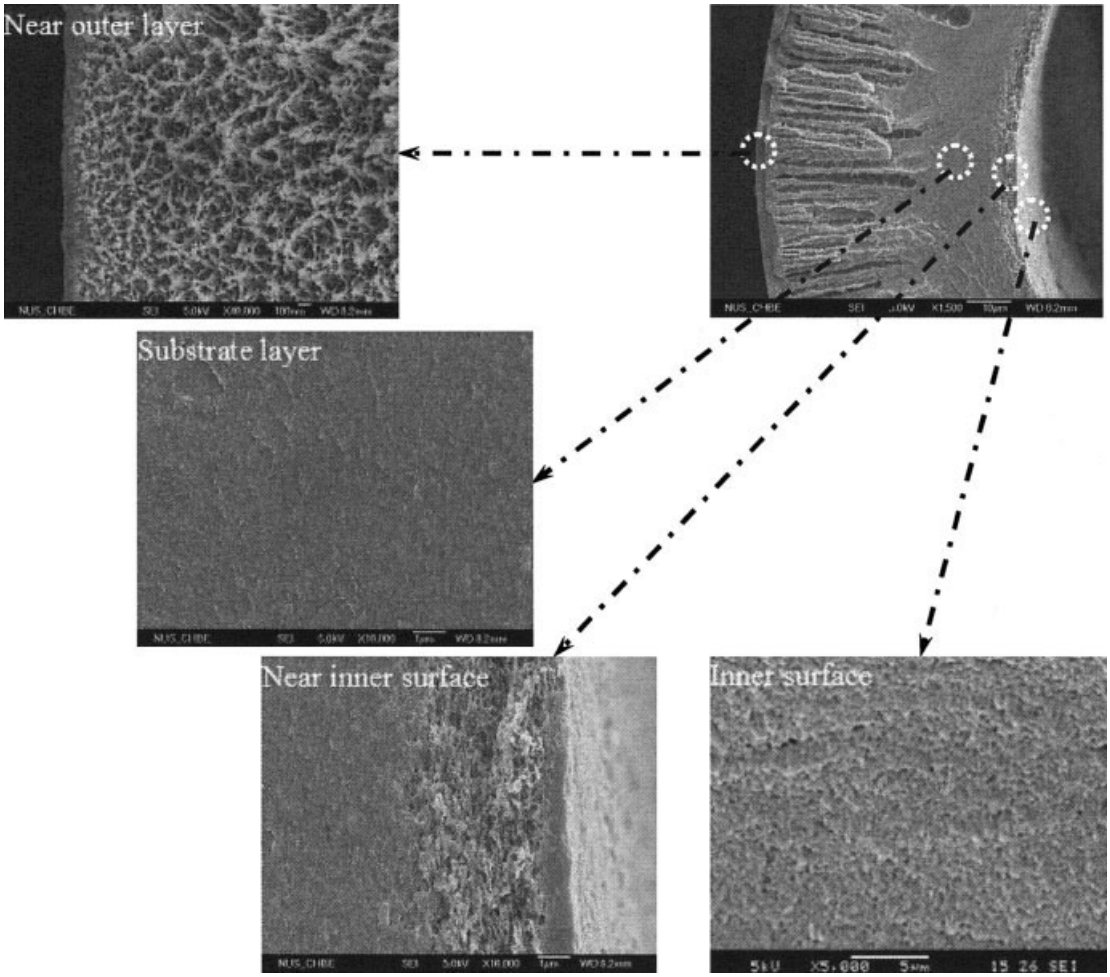

Figure 8. Cross section of PBI NF hollow-fiber membrane (Batch IV–E).

Bore fluid: ethylene glycol/DMAc 50/50 wt %; dope flow rate: 4.0 mL/min; elongational draw ratio φ: 13.74.

mixture, and a rapid phase inversion and membrane shrinkage occurring at the outer skin. A high bore-fluid flow rate may induce solvent intrusion, whereas a delayed demixing may result in a soft nascent skin that is vulnerable to stress imbalance and solvent intrusion. The water-induced rapid phase inversion and shrinkage at the outer membrane skin may produce additional inward hoop stress, which facilitates the intrusion of bore fluid into hollow fibers. As a consequence, the resultant PBI hollow-fiber membrane is full of fingerlike macrovoids and can withstand transmembrane pressures only up to 10 bar. The pure water permeability of this PBI hollow fiber is in the range of $5.18-6.95 \times 10^{-9}$ m^3 m^{-2} kPa^{-1} s^{-1} (1.5–2.5 L m^{-2} bar^{-1} h^{-1}), which is less than that [that is, 9.94×10^{-9} m^3 m^{-2} kPa^{-1} s^{-1} (3.58 L m^{-2} bar^{-1} h^{-1})] of a flat-sheet composite PBI membrane cast on the polyester nonwoven fabric from the same PBI polymer solution.

Following a previous practice to prepare PBI hollow-fiber membranes for reverse osmosis,[55] a nonsolvent, dodecane, was used as the bore fluid to fabricate PBI NF membranes. Dodecane is an inert hydrocarbon liquid that is immiscible with both DMAc (the spinning solvent) and water (the external coagulant). Figure 5 illustrates the resultant morphology. Clearly, dodecane and DMAc/water mixture produce PBI hollow-fiber membranes with different morphologies. This may arise from the fact that dodecane is an inert hydrocarbon liquid that is immiscible with the spinning solution. As a result, large fingerlike macrovoids are fully suppressed and a much denser structure with scattered tiny pores is formed in the cross section near the inner skin. However, a layer of small and elongated fingerlike macrovoids can be observed near the outer layer, possibly arising from water intrusion during the phase inversion. These PBI hollow-fiber membranes can withstand transmembrane pressures up to 30 bar with a pure water permeability of about $1.11-3.06 \times 10^{-9}$ m^3 m^{-2} kPa^{-1} s^{-1} (0.40–1.10 L m^{-2} bar^{-1} h^{-1}). Because the removal of dodecane from these hollow fibers is not a trivial process and the pure water permeability is just about the average, attention is given to other bore fluid chemistry.

Figures 6 and 7 show the morphology of PBI hollow-fiber membranes using 80/20 and 50/50 wt % ethylene glycol/DMAc mixtures as bore fluids, respectively. Similar to the dodecane case, an array of very small but elongated fingerlike macrovoids is formed near the outer layer, whereas the cross section near the inner skin seems to be a dense spongy structure. The inner skin appears to be relatively dense. This dense inner substructure morphology may be explained by the fact

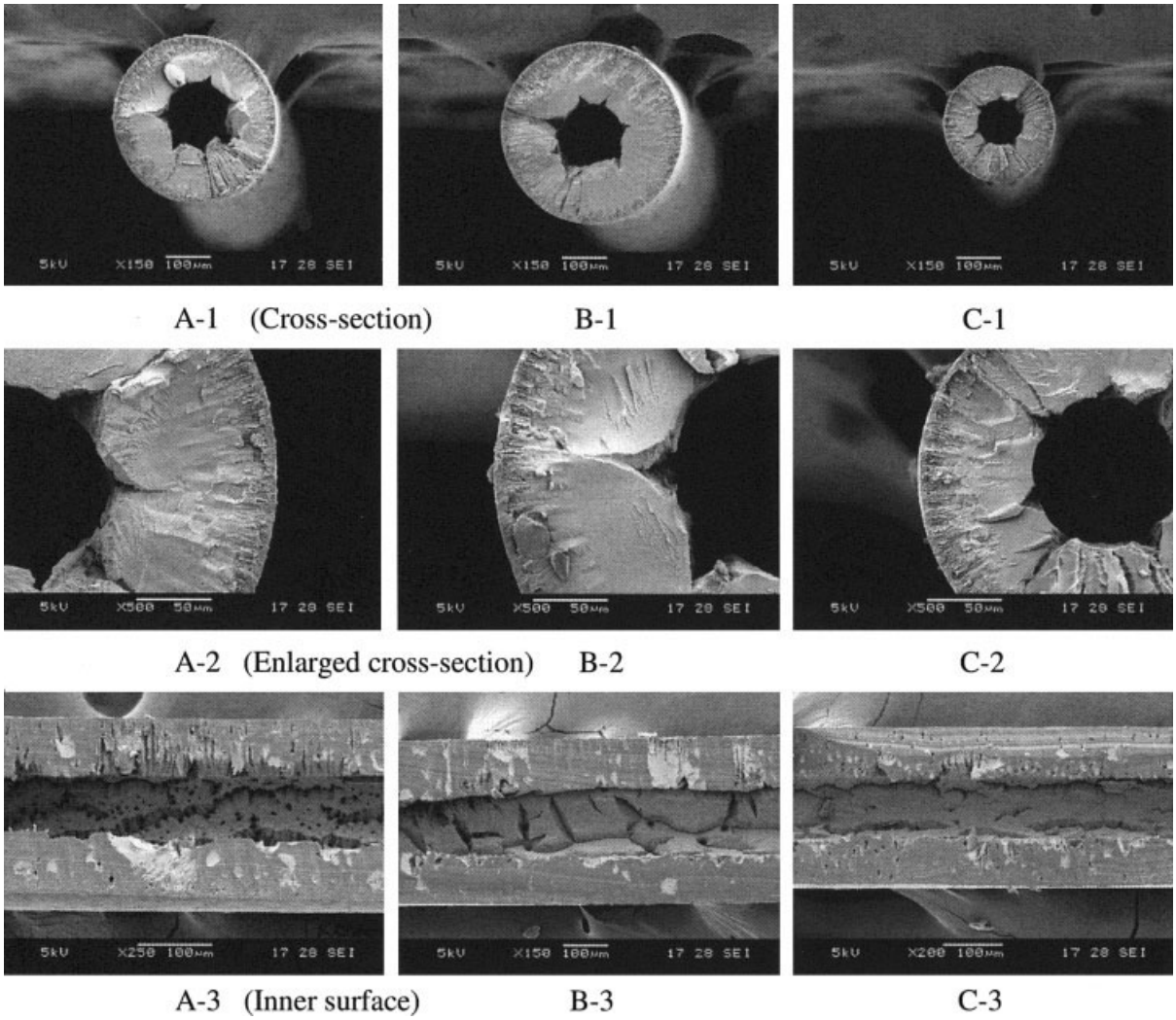

Figure 9. Effects of dope flow rate and elongation rate on the membrane structure of PBI NF hollow-fiber membranes from Batch V.

Bore fluid: ethylene glycol 23.3 wt %, DMAc 76.7 wt %.

that ethylene glycol is highly viscous and is inert to the PBI solution. High viscosity may retard the intrusion of ethylene glycol into the hollow fiber, whereas inertness cannot induce much phase separation.

When the content of DMAc in the bore fluid was increased to 50 wt %, the macroscopic morphology of the resultant membranes shown in Figure 7 seems to remain the same as that of membranes prepared in Batch III. However, the enlarged pictures illustrated in Figures 7 and 8 indicate a porous inner skin and a porous substructure underneath. If the DMAc content in the bore fluid was further increased to 76.7 wt % (Batch V), the integrity of hollow-fiber membranes deteriorated during the sample drying for SEM, as displayed in Figure 9. This phenomenon is a result of many factors: (1) the rich DMAc bore fluid may result in delayed mixing and form a very porous but weak nascent inner layer; (2) the imbalance of shrinkages across the membrane induces extra stresses for cracking during drying of the sample; and (3) the hydrophilic nature of phase-inversion PBI membranes, which absorb a substantial amount of water, leads to low mechanical properties after drying.[56]

Apart from Batches I and V, wet PBI hollow fibers fabricated from Batch II, Batch III, and Batch IV conditions can withstand higher operation pressures up to 30 bar. Because Batch IV conditions produce fibers with more desirable inner skin morphology than that of other conditions, PBI hollow-fiber membranes spun from Batch IV conditions were further studied for nanofiltration.

Effect of elongational rate on the mean pore size and pure water permeability

For PBI NF hollow fibers fabricated in Batch IV, the solute rejection vs. solute Stokes radius curves are plotted on a log-normal probability graph at the pressure of 20 bar, as illustrated in Figure 10. By fitting Eq. 2, straight-line relationships are obtained with reasonably high correlation coefficients ($r^2 > 0.96$). Table 3 lists the mean effective pore size μ_p at $R_T = 50\%$, and σ_p, the geometric standard deviation about μ_p, calculated from the plots. The MWCO (the molecular weight of solute at $R_T = 90\%$) can also be calculated from these

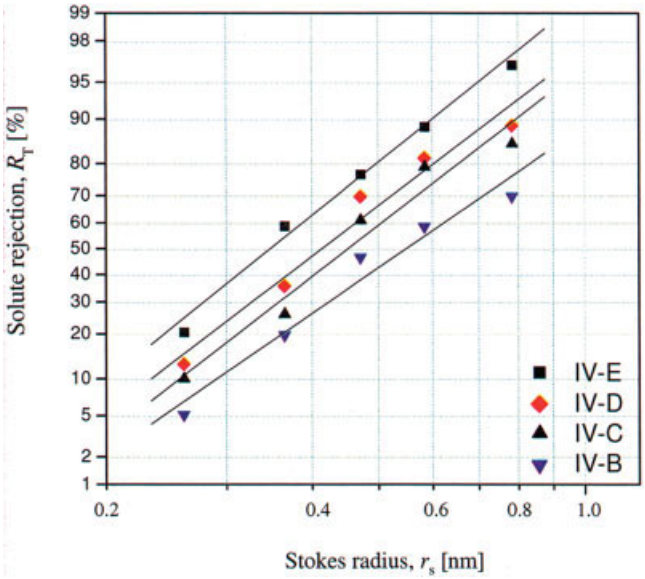

Figure 10. Effective rejection curves (solute rejections vs. their Stokes radii) plotted on the log-normal probability coordinate system for PBI NF hollow fibers spun at different elongation rates.

Testing pressure: 20 bar. [Color figure can be viewed in the online issue, which is available at www.interscience.wiley.com.]

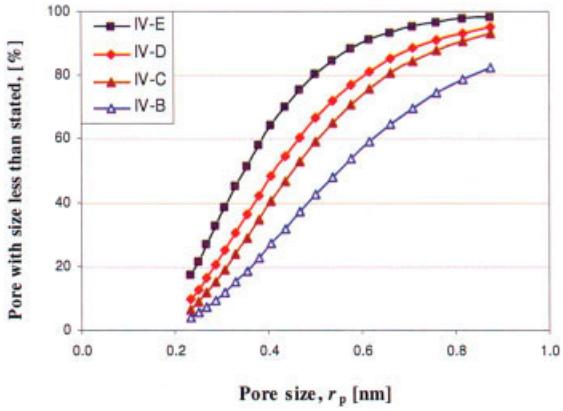

Figure 11. Cumulative pore size distribution curves of the PBI NF hollow-fiber membranes spun at different elongation rates.

[Color figure can be viewed in the online issue, which is available at www.interscience.wiley.com.]

straight lines and Eq. 4. The pore size distributions of the PBI membranes calculated from Eqs. 1 and 3 are depicted in Figures 11 and 12. It can be seen that the pore size distribution becomes narrow with increasing elongational rate. From Table 3, it is found that the pure water permeability increases, whereas the mean effective pore radius decreases, when increasing the elongational rate at the same dope flow rate. The results appear to confirm that the macromolecular packing and orientation induced by elongation stress intensively influence the phase-inversion process,[57] although the microstructure transformation cannot be visibly detected from SEM observation. Because surface pores are considered as the interstices among nodules, the elongation stress may elongate the nodule dimension as well as deaggregate nodules. The former may result in better packing and decrease in pore size, whereas the latter may increase in surface porosity.

Ion separation and surface charge property of the PBI NF hollow fiber using single-electrolyte solutions

In the following sections, the characterizations of ion separation performance and surface charge property of PBI NF hollow-fiber membranes IV–E are performed. These NF hollow fibers have a mean effective pore size of 0.348 nm in radius and a PWP of 5.18×10^{-9} m^3 m^{-2} kPa^{-1} s^{-1} (1.86 L m^{-2} bar^{-1} h^{-1}).

Because the PBI NF membranes seem to be positively charged at pH 7.0, they may show different rejections to various valent cations and anions. At the same molar concentration (3.4 mol m^{-3}), rejections of four types of single electrolytes in their solutions were measured at different pressures, as shown in Figure 13. They follow the order of R_T ($MgCl_2$) > R_T ($MgSO_4$) > R_T (Na_2SO_4) > R_T (NaCl). Interestingly, the PBI membranes exhibit the highest rejection to divalent cations but lower rejection to divalent anions, but the lowest rejection to monovalent ions. This phenomenon seems to deviate from the Donnan exclusion mechanism, which has also been observed elsewhere.[58,59] In addition, the solute rejection increases with increasing pressures. This can be explained by the fact that the water permeate flux through the membrane is linearly related to the applied pressure difference, whereas the solute flux is dependent on several factors: (1) the concentration gradient over the membrane; (2) the interaction between solute and fluid; and (3) the water permeate flux. As a result, when increasing the pressure difference, the water flux increases relatively faster than the solute flux,[60] which causes a decrease in solute permeate concentration and an increase in solute rejection.

Table 3. Hollow-Fiber Membrane Dimensions, Pure Water Permeability (PWP), Mean Effective Pore Size (μ_p), Geometric Standard Deviation (σ_p) and the Molecular Weight Cutoff (MWCO) of PBI Nanofiltration Hollow Fibers Spun from Batch IV

Fiber ID	Dope Flow Rate (mL min^{-1})	ID (μm)	OD (μm)	Elongation Ratio, φ	PWP $\times 10^{-9}$* (m^3 m^{-2} kPa^{-1} s^{-1})	r_p (nm)	σ_p	MWCO (Da)
IV–B	4.0	280	640	3.59	2.08	0.550	1.64	1778
IV–C	4.0	220	500	5.90	2.78	0.453	1.55	1016
IV–D	4.0	180	420	8.26	3.94	0.413	1.57	853
IV–E	4.0	160	335	13.74	5.18	0.348	1.53	551

*PWP for hollow fiber IV–B = 2.08×10^{-9} m^3 m^{-2} kPa^{-1} s^{-1}.

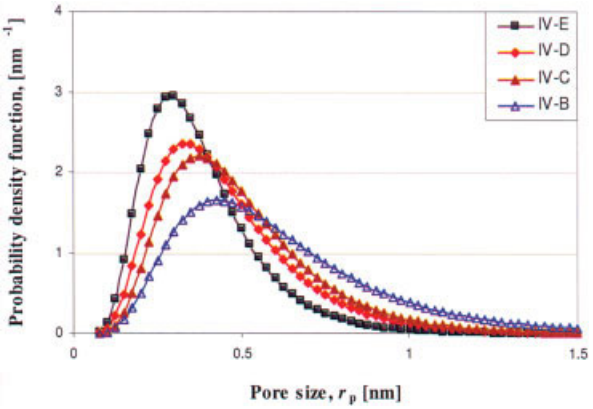

Figure 12. Probability density function curves of the PBI NF hollow-fiber membranes spun at different elongation rates.

[Color figure can be viewed in the online issue, which is available at www.interscience.wiley.com.]

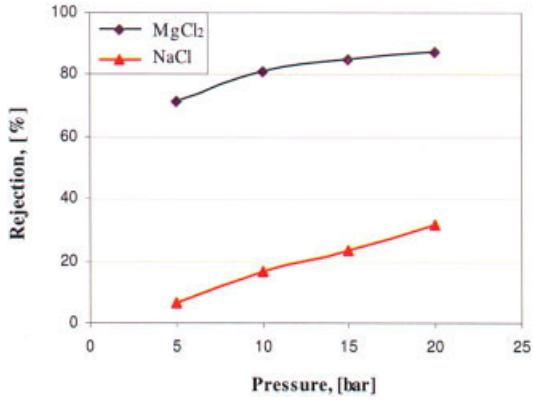

Figure 14. Ion rejection in the mixture of NaCl/$MgCl_2$ solution as a function of applied pressure.

[NaCl] = 3.4 mol m^{-3}, [$MgCl_2$] = 3.4 mol m^{-3}, pH 7.0. [Color figure can be viewed in the online issue, which is available at www.interscience.wiley.com.]

Ion fractionation by PBI NF membranes in the electrolyte mixture solutions

Generally, most electrolyte solutions may contain several salts that need to be separated through the membrane process. In this section, two kinds of binary salt mixtures were used to test the ion fractionation performance of the as-spun PBI NF membrane. For example, as shown in Figure 14, a NaCl/$MgCl_2$ binary salt solution (at pH 7.0) with a cation molar concentration ratio Na^+/Mg^{2+} of 1.0, Na^+ ions are forced to permeate preferentially compared to Mg^{2+} ions, given that Na^+ ions have lower valence and smaller hydrated ionic size than those of Mg^{2+} ions. Cl^- ions also permeate membrane together with Na^+ to maintain electroneutrality at both sides of the membrane phase in accordance with the Donnan principle. As a result, Mg^{2+} ions and Na^+ ions could be fractionated by the PBI NF membranes because of ion competition. In addition, along with an increase in pressure, the rejection of Mg^{2+} and Na^+ increases because an increase in water permeate flux results in a decrease in permeate concentration.

Similarly, as shown in Figure 15, in the NaCl/Na_2SO_4 binary salt solution (at pH 7.0) with an anion molar concentration ratio Cl^-/SO_4^{2-} of 1.0, Cl^- ions are forced to permeate preferentially compared to SO_4^{2-} ions because Cl^- has a lower valence and smaller hydrated ionic size. Na^+ ions also permeate the membrane together with Cl^- to maintain electroneutrality at both sides of the membrane phase, in accordance with the Donnan exclusion principle. Moreover, the negative rejection (the Cl^- concentration in permeate is more than that in feed solution) of chloride ions is observed at different pressures. Along with an increase in pressure, the rejection of SO_4^{2-} increases, whereas the rejection of Cl^- first decreases to a minimum, then increases. Clearly, SO_4^{2-} ions and Cl^- ions could be fractionated by the charged PBI NF membranes.

However, it is still not clear why the PBI NF membranes exhibit higher rejection to both divalent cations and divalent

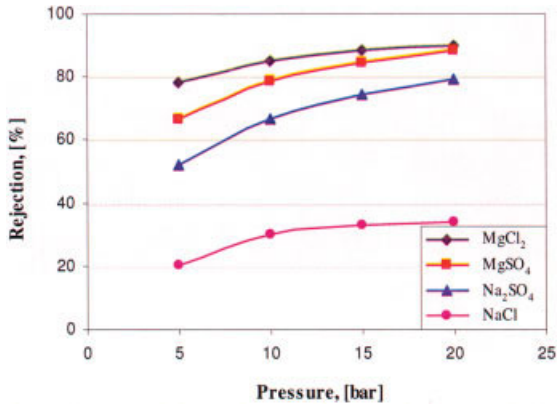

Figure 13. Rejection of different single salts as a function of different pressure.

The bulk single salt concentration: 3.4 mol m^{-3}, pH 7.0. [Color figure can be viewed in the online issue, which is available at www.interscience.wiley.com.]

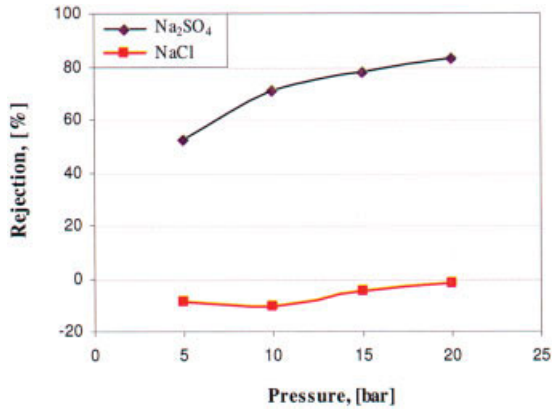

Figure 15. Ion rejection in the mixture of NaCl/Na_2SO_4 solution as a function of applied pressure.

[NaCl] = 3.4 mol m^{-3}, [Na_2SO_4] = 3.4 mol m^{-3}, pH 7.0. [Color figure can be viewed in the online issue, which is available at www.interscience.wiley.com.]

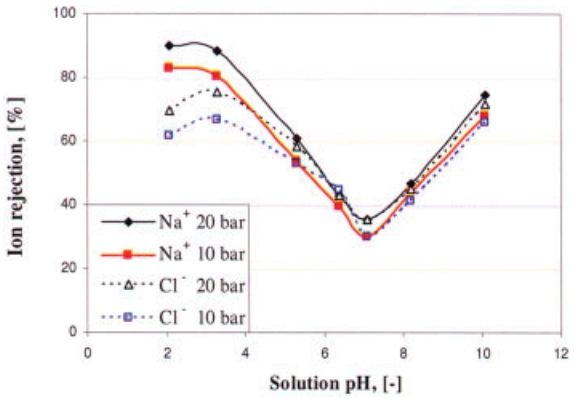

Figure 16. Rejection of NaCl (3.4 mol m^{-3}, 20°C) as a function of solution pH under different pressures.

Solution pH was adjusted by adding 1.0 N HCl or 1.0 N NaOH. [Color figure can be viewed in the online issue, which is available at www.interscience.wiley.com.]

anions compared to monovalent ions at pH 7.0. The possible explanation may arise from the existence of an amphoteric imidazole group within PBI molecules.

Effects of solution pH on NaCl rejection

The separation performance of the PBI NF membrane largely depends on the surface charge, which is influenced by pH of the contacted media. A V-shape trend of NaCl rejection, shown in Figure 16, reflects the surface charge property under different pH values. A minimum ion rejection appears at pH 7.0 (near pK_a of the imidazole group in PBI molecules). This result seems to be similar to the amphoteric behavior of metal oxide group of the inorganic membranes under different pH values.[61] It is possible to speculate that the PBI membranes have different charge signs based on pH values of the media (that is, positively charged at lower pH and negatively charged at higher pH). It is also found that at very low pH (pH $\simeq$ 2.0) the rejection of Cl^- decreases, whereas rejection of Na^+ increases along with a decrease in pH. Because HCl solution was used to adjust the pH of NaCl solution, the NaCl solution contains Na^+, Cl^-, and substantialy more H^+ ions (10 mol m^{-3}) at pH 2.0. As compared to Na^+, H^+ can preferably permeate through the membrane, and Cl^- comes together with H^+ to maintain the electroneutrality of solutions. Thus, at pH 2.0, the PBI membrane shows lower rejection of Cl^- but higher rejection of Na^+.

Cephalexin separation performance of PBI NF hollow-fiber membranes

As an amphoteric electrolyte molecule in the aqueous solution, cephalexin acts as both base (proton acceptor) and acid (proton donor), given that cephalexin molecules have both the amino group ($-NH_2$) and the carboxyl group (–COOH) similar to amino acids. Depending on the pH of solution, cephalexin can be positively charged (acidic) at pH $<$ pI (isoelectric point $\simeq$ 4.5–5.0), negatively charged (basic) at pH $>$ pI, and net neutral (dipolarions) at pH = pI. In the dipolar form, the amino group is protonated ($-NH_3^+$) and the carboxyl group is dissociated ($-COO^-$).[29] Based on their dissociation constants (pK_a values), the fraction of different ionization state of cephalexin at different pH values can be expressed by the Henderson–Hasselbalch equation[62] plotted in Figure 17 (blue curves):

$$\mathrm{pH} = \mathrm{p}K_a + \log\left(\frac{[\text{proton acceptor}]}{[\text{proton donor}]}\right) \tag{8}$$

As shown in Figure 17, the rejection of cephalexin by PBI NF membrane shows a V-shape trend with increasing pH at different pressures and a minimum rejection appears at pH $\simeq$ 5.0 (near pI of cephalexin molecules).

Although cephalexin has almost the same molecular weight with saccharose, the rejection of cephalexin (~86.5%) at pH values around the pI (4.5–5.0; which cephalexin molecules as a whole is zwitterion without net charge) is higher than that of saccharose (~76.8%). This may arise from the contribution of molecular shape to the solute transport.[63] By taking the molecular configuration into account, the cephalexin molecule is more like a rod with the length of 1.6 nm away from a sphere and the saccharose molecule is 1.2 nm in length, whereas their molecular widths are quite close, which are simulated from *Cerius*2 molecular simulation software[64] shown in Figure 18. Therefore, the steric hindrance for cephalexin may be much greater than that of saccharose. However, as a dipolar ion with two opposite charged sites, the rejection behavior of cephalexin at the state with no net charge is different from that of a neutral molecule.[65] The amino group ($-NH_3^+$) is repulsed by the positively charged membrane (at pH $<$ pK_a of PBI), whereas the carboxyl group ($-COO^-$) is attracted by the membrane. Thus, cephalexin molecules are aligned along the axial direction of pores under convection, which could make cephalexin rejection decrease. As a result, at a pH near the pI of cephalexin, steric exclusion plays a main role in the rejection of cephalexin.

These results confirm that the rejection of cephalexin is dependent on the pore size (steric exclusion) and the electrostatic interaction between solutes and membrane. The solution pH has the dominant effect on the separation of cephalexin because pH determines the ionization states of the cephalexin molecules and surface charge characteristics of the PBI membranes.

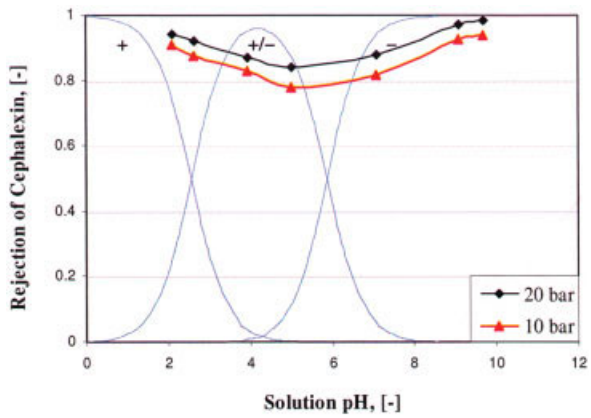

Figure 17. Rejection of cephalexin (200 ppm) vs. the solution pH under different pressures.

[Color figure can be viewed in the online issue, which is available at www.interscience.wiley.com.]

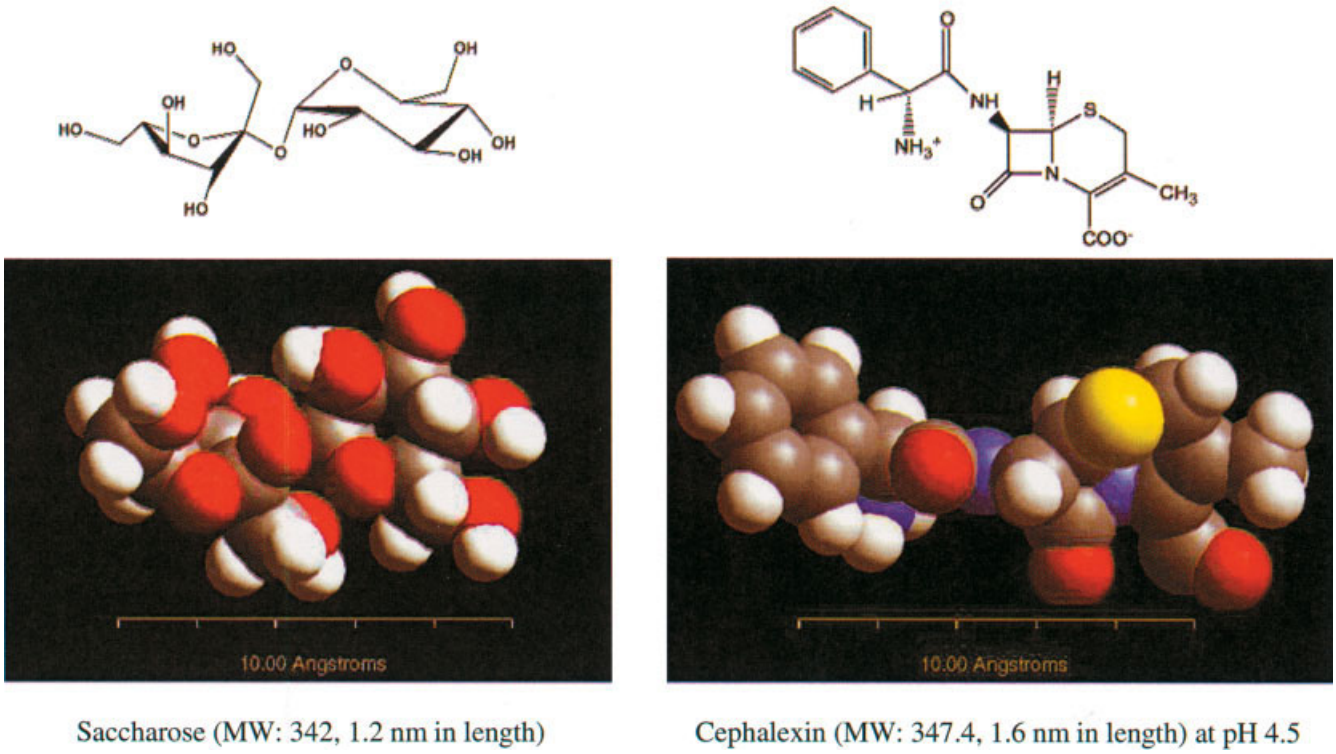

Figure 18. Molecular configurations simulated from *Cerius*2.

[Color figure can be viewed in the online issue, which is available at www.interscience.wiley.com.]

Conclusions

High-pressure sustainable PBI nanofiltration hollow-fiber membranes have been fabricated through the phase-inversion process. Because of the strong interaction between PBI and water, the formation of fingerlike macrovoids inside the PBI hollow fiber cannot be avoided when water was used as the external coagulant. However, by using a mixture of ethylene glycol and DMAc as the bore fluid solution, the macrovoid-free formation can be produced in the inner substrate of PBI hollow-fiber membranes. The resultant PBI NF hollow fibers can withstand higher pressures up to 30 bar.

PBI NF hollow-fiber membranes spun from Batch IV–E have a mean effective pore size of 0.348 nm in radius and a narrow pore size distribution. They show higher rejection to divalent cations, lower rejection to divalent anions, and the lowest rejection to monovalent ions, which seems not to be correlated with the Donnan exclusion mechanism, whereas for the binary NaCl/Na_2SO_4 mixture solution, the negative rejection of Cl^- and high rejection of SO_4^{2-} can be explained by the ion competing transport mechanism. In addition, in the binary NaCl/$MgCl_2$ mixture solution, PBI membrane exhibits a much higher rejection of Mg^{2+} over Na^+. Thus, divalent ions and monovalent ions can be effectively fractionated in their mixtures by the PBI membrane.

Based on the amphoteric property of PBI molecules, the PBI membrane shows a V-shape trend of NaCl rejection under different pH values, which is attributed to the surface charge characteristics influenced by solution pH. The newly developed PBI NF membranes can concentrate and purify cephalexin from aqueous solutions by adjusting operation conditions based on the interaction between the charged membrane surface and the ionized cephalexin molecules under different pH values.

Acknowledgments

The authors thank the National University of Singapore (NUS) for funding this project under Grant R-279-000-165-112.

Notation

A = effective filtration area of membrane, m^2
C_{feed} = solute concentration in the feed solution, mol m^{-3}
$C_{permeate}$ = solute concentration in the permeate, mol m^{-3}
D_s = diffusivity of solute in the solution, m^2 s^{-1}
ID = inner diameter, μm
MWCO = molecular weight cutoff, Da
MW = molecular weight, Da
M_W = weight average molecular weight, Da
OD = outer diameter, μm
pI = isoelectric point
pK_a = ionization equilibrium constant
PWP = pure water permeability, m^3 m^{-2} kPa^{-1} s^{-1}
Q = water permeation volumetric flow rate, m^3 s^{-1}
r_s = solute Stokes radius, nm
r_p = effective pore radius, nm
R_T = effective solute rejection
u_f = linear velocity of feed stream, m s^{-1}
ΔP = trans-membrane pressure drop, kPa
μ_p = mean effective pore radius, nm
μ_s = geometric mean radius of solute at R_T = 50%, nm
σ_g = geometric standard deviation about μ_s
σ_p = geometric standard deviation about μ_p
φ = elongational draw ratio

Literature Cited

1. Raman LP, Cheryan M, Rajagopalan N. Consider nanofiltration for membrane separations. *Chem Eng Prog.* 1994;90:68-74.
2. Sirkar KK. Membrane separation technologies: Current developments. *Chem Eng Commun.* 1997;157:145-184.
3. Donnan FG. Theory of membrane equilibria and membrane potentials

in the presence of non-dialysing electrolytes. A contribution to physical-chemical physiology. *J Membr Sci.* 1995;100:45-55.
4. Yaroshchuk AE. Rejection mechanisms of NF membranes. *Membr Technol.* 1998;100:9-12.
5. Perry M, Linder C. Intermediate reverse osmosis ultrafiltration (RO UF) membranes for concentration and desalting of low molecular weight organic solutes. *Desalination.* 1989;71:233-245.
6. Watson BM, Hornburg CD. Low energy membrane nanofiltration for removal of color organic and hardness from water supplies. *Desalination.* 1989;72:11-22.
7. Vrijenhoek EM, Waypa JJ. Arsenic removal from drinking water by a "loose" NF membrane. *Desalination.* 2000;130:265-276.
8. Horst HC, Timmer JM, Robbertsen T, Leenders J. Use of nanofiltration for concentration and demineralization in the dairy industry: Model for mass transport. *J Membr Sci.* 1995;104:205-218.
9. Whu JA, Baltzis BC, Sirkar KK. Modeling of nanofiltration-assisted organic synthesis. *J Membr Sci.* 1999;163:319-331.
10. Christy C, Vermant S. The state-of-the-art of filtration in recovery processes for biopharmaceutical production. *Desalination.* 2002;147: 1-4.
11. Capelle N, Moulin P, Charbit F, Gallo R. Purification of drug derivative from concentrated saline solution by nanofiltration. *J Membr Sci.* 2002;196:125-141.
12. Sheth JP, Qin Y, Sirkar KK, Baltzis BC. Nanofiltration-based diafiltration process for solvent exchange in pharmaceutical manufacturing. *J Membr Sci.* 2003;211:251-261.
13. Paul EL, Rosas CB. Challenges for chemical engineers in the pharmaceutical industry. *Chem Eng Prog.* 1990;86:17-25.
14. Rautenbach R, Groschl A. Separation potential of NF membranes. *Desalination.* 1990;77:73-84.
15. Tsuru T, Shutou T, Nakao SI, Kimura S. Peptide and amino acid separation with NF membranes. *Sep Sci Technol.* 1994;29:971-984.
16. Wang XL, Ying AL, Wang WN. Nanofiltration of L-phenylalamine and L-aspartic acid aqueous solutions. *J Membr Sci.* 2003;196:59-67.
17. Mahon HI. *Permeability Separatory Apparatus and Process Using Hollow Fibers*. U.S. Patent No. 3 228 877; 1966.
18. Yang C, Cussler EL. Reactive extraction of penicillin G in hollow-fiber and hollow-fiber fabric modules. *Biotechnol Bioeng.* 2000;69:66-73.
19. Strathmann H. Membrane separation processes: Current relevance and future opportunities. *AIChE J.* 2001;47:1077-1087.
20. Petersen RJ. Composite reverse osmosis and nanofiltation membranes. *J Membr Sci.* 1993;83:81-150.
21. Weber R, Chmiel H, Mavrov V. Characteristics and application of ceramic NF membranes. *Ann NY Acad Sci.* 2003;984:178-193.
22. Chung TS. Polybenzimidazoles. In: Olabisi O, ed. *Handbook of Thermoplastics*. New York, NY: Marcel Dekker; 1997:701-732.
23. Kreuer KD, Fuchs A, Ise M, Spaeth M, Maier J. Imidazole and parazole-based proton conducting polymers and liquids. *Electrochim Acta* 1998;43:1281-1288.
24. Staiti P, Lufrano F, Aricò AS, Passalacqua E, Antonucci V. Sulfonated polybenzimidazole membranes—Preparation and physico-chemical characterization. *J Membr Sci.* 2001;188:71-78.
25. Samms SR, Wasmus S, Savinell RF. Thermal stability of proton conducting acid doped polybenzimidazole in simulated fuel cell environments. *J Electrochem Soc.* 1996;143:1225-1232.
26. Bouchet R, Siebert E. Proton conduction in acid doped polybenzimidazole. *Solid State Ionics.* 1999;118:287-299.
27. Glipa X, Bonnet B, Mula B, Jones DJ, Roziere J. Investigation of the conduction properties of phosphoric and sulfuric acid doped polybenzimidazole. *J Mater Chem.* 1999;9:3045-3049.
28. Maladkar NK. Enzymatic production of cephalexin. *Enzyme Micro Technol.* 1994;16:715-718.
29. Sahoo GC, Ghosh AC, Dutta NN. Recovery cephalexin from dilute solution in a bulk liquid membrane. *Proc Biochem.* 1997;32:265-272.
30. Bowen WR, Mohammed AW, Hilal N. Characterization of NF membranes for predictive purposes—Use of salts, uncharged solutes and atomic force microscopy. *J Membr Sci.* 1997;126:91-105.
31. Singh S, Khulbe K, Matsuura T, Ramamurthy P. Membrane characterization by solute transport and atomic force microscopy. *J Membr Sci.* 1998;142:111-127.
32. Michaels AS. Analysis and prediction of sieving curves for ultrafiltration membranes: A universal correlation. *Sep Sci Technol.* 1980;15: 1305-1322.
33. Aimar P, Meireles M, Sanchez V. A contribution to the translation of retention curves into pore size distribution for sieving membranes. *J Membr Sci.* 1990;54:321-338.
34. Youm KH, Kim WS. Prediction of intrinsic pore properties of ultrafiltration membrane by solute rejection curves: Effects of operating conditions on pore properties. *J Chem Eng Jpn.* 1991;24:1-7.
35. Bowen WR, Mohammad AW. Characterization and prediction of NF membrane performance—A general assessment. *Trans IChemE A.* 1998;76:885-893.
36. Wang KY, Chung TS. The characterization of flat composite NF membranes and their applications in the separation of cephalexin. *J Membr Sci.* 2004;247:37-50.
37. Mulder M. *Basic Principles of Membrane Technology*. Dordrecht, The Netherlands: Kluwer Academic; 1996.
38. Li DF, Chung TS, Ren JZ, Wang R. Thickness dependence of macrovoids evolution in wet phase-inversion asymmetric membranes. *Ind Eng Chem Res.* 2004;43:1553-1556.
39. Wang KY, Li DF, Chung TS, Chen SB. The observation of elongation dependent macrovoid evolution in single- and dual-layer asymmetric hollow fiber membranes. *Chem Eng Sci.* 2004;59:4657-4660.
40. McHugh AJ, Yilmaz L. The diffusion equation for polymer membrane formation in ternary systems. *J Polym Sci Part B: Polym Phys.* 1985;23:1271-1274.
41. Smolders CA, Reuvers AJ, Boom RM, Wienk IM. Microstructures in phase-inversion membranes. Part 1. Formation of macrovoids. *J Membr Sci.* 1992;73:259-275.
42. Strathmann H, Kock K, Amar P, Baker RW. The formation mechanism of asymmetric membranes. *Desalination.* 1975;16:179-203.
43. Shojaie SS, Krantz WB, Greenberg AR. Dense polymer film and membrane formation via the dry-cast process. II. Model validation and morphological study. *J Membr Sci.* 1994;94:281-298.
44. Chung TS, Hu XD. Effect of air-gap distance on the morphology and thermal properties of polyethersulfone hollow fibers. *J Appl Polym Sci.* 1997;66:1067-1077.
45. Pekny MR, Zartman J, Krantz WB, Greenberg AR, Todd P. Flow-visualization during macrovoid pore formation in dry-cast cellulose acetate membranes. *J Membr Sci.* 2003;211:71-90.
46. Levich VG, Krylov VS. Surface tension driven phenomena. *Annu Rev Fluid Mechanics.* 1969;1:293-316.
47. McKelvey SA, Koros WJ. Phase separation, vitrification, and the manifestation of macrovoids in polymeric asymmetric membranes. *J Membr Sci.* 1996;112:29-39.
48. Kesting RE, Fritzsche AK. *Polymeric Gas Separation Membranes*. New York, NY: Wiley; 1993.
49. Boom RM, Wienk IM, van den Boomgaard Th, Smolders AA. Microstructures in phase inversion membranes. Part 2. The role of a polymeric additive. *J Membr Sci.* 1992;73:277-292.
50. Ren JZ, Chung TS, Li DF, Wang R, Liu Y. Development of asymmetric 6FDA-2, 6 DAT hollow fiber membranes for COB_{2B}/CHB_{4B} separation. 1. The influence of dope composition and rheology on membrane morphology and separation performance. *J Membr Sci.* 2002;207:227-240.
51. Kim JH, Min BR, Won J, Park HC, Kang YS. Phase behavior and mechanism of membrane formation for polyimide/DMSO/water system. *J Membr Sci.* 2001;187:47-55.
52. Lin KY, Wang DM, Lai JY. Nonsolvent-induced gelation and its effect on membrane morphology. *Macromolecules.* 2002;35:6697-6706.
53. Tsai HA, Li LD, Lee KR, Wang YC, Li CL, Huang J, Lai JY. Effect of surfactant addition on the morphology and pervaporation performance of asymmetric polysulfone membranes. *J Membr Sci.* 2000; 176:97-103.
54. Li DF, Chung TS, Wang R. Morphology aspects and structure control of dual-layer asymmetric hollow fiber membranes formed by a simultaneous co-extrusion approach. *J Membr Sci.* 2004;243:155-175.
55. Model FS, Davis HJ, Poist JE. PBI membrane for reverse osmosis. In: Sourirajan S, ed. *Reverse Osmosis and Synthetic Membranes—Theory, Technology, Engineering*. Ottawa, Canada: National Research Council; 1977:231-248.
56. Chung TS. A critical review of polybenzimidazoles: Historical development and future R&D. *J Macromol Sci Polym Rev.* 1997;C37:277-301.
57. Chung TS. The limitations of using Flory–Huggins equation for the states of solutions during asymmetric hollow fiber formation. *J Membr Sci.* 1997;126:19-34.

58. Schaep J, Van der Bruggen B, Vandecasteele C, Wilms D. Influence of ion size and charge in nanofiltration. *Sep Purif Technol.* 1998;14:155-162.
59. Yaroshchuk AE. Dielectric exclusion of ions from membranes. *Adv Colloid Interface Sci.* 2000;85:193-230.
60. Garcia-Aleman J, Dickson JM. Mathematical modeling of NF membranes with mixed electrolyte solutions. *J Membr Sci.* 2004;235:1-13.
61. Guizard C, Rios G. Transport and fouling phenomena in liquid phase separation with inorganic and hybrid membranes. In: Burggraaf AJ, Cot L, eds. *Fundamentals of Inorganic Membrane Science and Technology*. Amsterdam, The Netherlands: Elsevier Science; 1996:569-618.
62. Stryer L. *Biochemistry*. 4th Edition. New York, NY: W. H. Freeman; 1995.
63. Kiso Y, Kon T, Kitao T, Nishimura K. Rejection properties of alkyl phthalates with NF membranes. *J Membr Sci.* 2001;182:205-218.
64. *Cerius2 Simulation Tool User's Reference: Molecular Simulations Software for Material Science*. San Diego, CA: Accelrys, Molecular Simulation Inc.; 2001.
65. Martin-Orue C, Bouhallab S, Garem A. Nanofiltration of amino acid and peptide solutions: Mechanisms of separation. *J Membr Sci.* 1998; 142:225-233.

Manuscript received May 21, 2005, and revision received Oct. 7, 2005.